JOURNAL OF GUIDANCE, CONTROL, AND DYNAMICS
Vol. 33, No. 4, July–August 2010

Initial Trajectory Model for a Multi-Maneuver Moon-to-Earth Abort Sequence

Cesar Ocampo* and Robin R. Saudemont†
University of Texas at Austin, Austin, Texas 78712

DOI: 10.2514/1.46955

To support the mission design and trajectory design problems associated with the moon-to-Earth trajectories for the crew exploration vehicle, a starting trajectory model that serves as the first iterate for a complete targeting and optimization procedure that takes a spacecraft from any closed lunar parking orbit to the Earth entry interface state for any date is developed. The motivation for this work is to examine the any-time abort capability required for human moon missions. The results presented here are limited to impulsive maneuvers. An analytical procedure is developed that constructs a multi-impulse escape trajectory from the moon propagated forward in time and a backward propagated trajectory from the Earth with a mismatch in position and velocity near the sphere of influence of the moon. The position and velocity discontinuities at the mismatch point are small enough to lie within the convergence envelope of a simple gradient based differential correction procedure that can, at a minimum, generate a feasible solution. This solution can then be analyzed further and serve as an initial estimate for an optimization procedure. The efficiency of the method is illustrated by solving any-time abort transfer problems typical for a human mission.

I. Introduction

AS PART of the requirements for a human lunar mission, a spacecraft on the surface of the moon must have the capability to safely return a human crew to the Earth in the case the mission has to be aborted. The constraints of such a mission require the ability to leave the moon and return to the Earth as soon as possible using the available propellent. This will often occur under unfavorable transEarth injection conditions, and thus significant plane changes will generally be required. Though it is always possible to escape a closed orbit for any given hyperbolic asymptote with a single maneuver, multiple-impulse maneuver sequences can yield considerable savings, in terms of Δv, especially when large plane changes are required [1].

The escape from a closed orbit about a central body to a constrained hyperbolic excess velocity vector has been studied in the past where single to multi-impulse escape sequences were examined. Gunther [2] examined one and two impulse escape and capture trajectories from and to a circular orbit about central body. The second impulse, assumed to occur at infinity or at the sphere of influence, provided the necessary plane change when the declination of the hyperbolic asymptote was above a critical value. Gerbracht and Penzo [3] examined optimal three-impulse escape sequences from an elliptical orbit to a hyperbolic excess velocity vector asymptote. An analytical model was used to construct the transfer sequence, which is then optimized using a numerical optimization procedure. Several families of solutions were found that were dependent on the eccentricity of the departure orbit and the relative declination of the hyperbolic asymptote. Bean [4] examined a similar three-impulse escape problem and applied it directly to a circular orbit escape from the Earth to hyperbolic excess velocity vector asymptotes typical of Earth-to-Mars trajectories. Again, an analytical procedure was used to construct the escape sequence which was then optimized using a numerical procedure. Edelbaum [5] examined the analytical optimization of a multimaneuver escape sequence from a given circular orbit to a hyperbolic excess velocity vector. The transfer time between the first and last maneuvers was held fixed. A key result concerned the existence of a fourth maneuver when the declination of the hyperbolic asymptote exceeded a critical value; below this critical value, three impulses or less are sufficient for an optimal escape sequence.

Given an epoch and an initial parking orbit at the moon, a vector based, analytical procedure is described here to generate a time free initial estimate for a complete moon-to-Earth return trajectory. This estimate produces a disconnected pair of trajectories that is then differentially corrected to guarantee continuity in time, position, and velocity. The results will show that the initial estimate is close to the final fully integrated solution and requires only a few iterations of the differential correction procedure. This feasible solution can then be further used as an initial estimate for a an optimization sequence. The optimization of this solution is not discussed here and forms part of current work. This analysis is applicable to all spacecraft missions that begin in a closed lunar orbit and are required to return to the Earth with specified Earth entry interface conditions. The main distinction between previous work and the current work is that here a complete, high-fidelity, lunar orbit to Earth transfer is generated consistent with the imposed constraints. If the current study was limited to constructing only the escape phase from a closed orbit about a central body to a given hyperbolic asymptote which is then optimized numerically, the performance results would be similar to the results reported by Gerbracht and Penzo [3], and Bean [4].

II. Description of the Problem

The problem is described as follows. Given an epoch, t_m, and the orbital elements of a closed (eccentricity, $e_0 < 1$) orbit around the moon, determine a maneuver transfer sequence that will take the spacecraft to the entry interface conditions at the Earth. The study is limited to examining only a subset of all the multimaneuver escape sequences that are possible. Two cases are examined that correspond to one or three transEarth injection (TEI) maneuvers. These are modeled as impulses. The main goal of the algorithm is to generate a feasible, high-fidelity, end-to-end lunar orbit to Earth transfer that serves as a starting iterate for further study, such as an optimization sequence for either impulsive and/or finite burn maneuvers. The

Received 31 August 2009; revision received 12 April 2010; accepted for publication 23 February 2010.

*Associate Professor, Department of Aerospace Engineering and Engineering Mechanics, W. R. Woolrich Laboratories, 1 University Station, C0600, 210 East 24th Street; cesar.ocampo@mail.utexas.edu.

†Graduate Student, Department of Aerospace Engineering and Engineering Mechanics, W. R. Woolrich Laboratories, 1 University Station, C0600, 210 East 24th Street; rsaudemont@mail.utexas.edu.

algorithm is robust and fast, and can be considered as an onboard program requiring limited computational capability.

At the Earth entry interface (EEI) point that occurs at t_e, the spacecraft state has to satisfy both lower and upper boundary constraints for a subset of the seven quantities that define the EEI state. These are the radial distance r (or altitude h), longitude λ, latitude ϕ, velocity magnitude v, flight-path angle ψ, azimuth γ, and the time t_e. Where applicable, these constraints can be expressed in either Earth fixed (nonrotating) or Earth body fixed (rotating) coordinates.

III. General Methodology

The overall solution procedure to the problem is divided into the following three major steps:

1) For a given set or subset of conditions on the Earth entry interface values and time epoch of the moon-centered orbit, t_m, compute in backward time a trajectory from the Earth to the moon. This backward trajectory is based on a Hohmann-type transfer, and it terminates at a preselected distance from the moon. A zero-sphere of influence model is used to construct this trajectory. The end state of this trajectory is transformed into a moon-centered state. From this, the target hyperbolic excess velocity vector with respect to the moon $\mathbf{v}_\infty^+$ for the departure orbit is obtained. The details of this step are described in Sec. V.

2) An analytical method is used to construct a one or three-impulse TEI sequence in moon-centered coordinates to achieve the $\mathbf{v}_\infty^+$ computed from step 1. The details of this step are described in Sec. IV.

3) A high-fidelity multibody gravitational model with numerical integration is used to construct two distinct trajectories. One is the impulsive moon-centered TEI sequence from step 2 and the other one is the Earth-to-moon backward integrated trajectory found in step 1. A match point is selected near the sphere of influence of the moon to end both trajectories. A minimum norm differential correction procedure is used to match continuity of time, position, and velocity at this patch point. The details of this step are described in Sec. VI.

IV. Construction of the Moon Escape Sequence

In a two-body force field, the parking orbit is defined in a fixed moon-centered frame, which serves as the basis for $\mathbf{v}_\infty^+$. This parking orbit around the moon is assumed to be closed (eccentricity, $e_0 < 1$). $\|\mathbf{v}_\infty^+\| > 0$ is required so that parabolic escape orbits are excluded. The parking orbit has angular momentum vector $\mathbf{h}_0$, and $\mathbf{h}_0$ and $\mathbf{v}_\infty^+$ are both normalized

$$\hat{\mathbf{h}}_0 = \frac{\mathbf{h}_0}{\|\mathbf{h}_0\|}, \qquad \hat{\mathbf{v}}_\infty^+ = \frac{\mathbf{v}_\infty^+}{\|\mathbf{v}_\infty^+\|} \tag{1}$$

A key part required for an initial estimate is obtaining the unit vector normal to the departure orbit plane described by the associated direction of the departure angular momentum vector, $\hat{\mathbf{h}}_f$. There are three subcases to consider:

1) $|\hat{\mathbf{h}}_0 \cdot \hat{\mathbf{v}}_\infty^+| = 0$ implies that $\hat{\mathbf{h}}_0$ is normal to $\hat{\mathbf{v}}_\infty^+$ and no plane change is required. The departure orbit plane can be coincident with the parking orbit plane, and is chosen to be so. In this case, their respective angular momentum vectors are collinear. There are two possible choices for $\hat{\mathbf{h}}_f$, $\hat{\mathbf{h}}_f = \pm\hat{\mathbf{h}}_0$. $\hat{\mathbf{h}}_f = +\hat{\mathbf{h}}_0$ is chosen for a zero angle plane change. The other choice requires a 180° plane change, which implies an expensive retrograde maneuver and is thus discarded.

2) $|\hat{\mathbf{h}}_0 \cdot \hat{\mathbf{v}}_\infty^+| = 1$ implies that $\hat{\mathbf{h}}_0$ is collinear with $\hat{\mathbf{v}}_\infty^+$; they are either in the same or opposite directions and a 90° plane change is required. The departure orbit plane is normal to the parking orbit plane. Any vector normal to $\hat{\mathbf{v}}_\infty^+$ can serve as $\hat{\mathbf{h}}_f$, which is also normal to $\hat{\mathbf{h}}_0$. Here, $\hat{\mathbf{h}}_f$ is chosen to be either

$$\hat{\mathbf{h}}_f = \pm\frac{\hat{\mathbf{h}}_0 \times \hat{\mathbf{r}}_{p_0}}{\|\hat{\mathbf{h}}_0 \times \hat{\mathbf{r}}_{p_0}\|} \tag{2}$$

or

$$\hat{\mathbf{h}}_f = \frac{\hat{\mathbf{r}}_{p_0} \times \hat{\mathbf{v}}_\infty^+}{\|\hat{\mathbf{r}}_{p_0} \times \hat{\mathbf{v}}_\infty^+\|} \tag{3}$$

where

$$\hat{\mathbf{r}}_{p_0} = \frac{\mathbf{r}_{p_0}}{r_{p_o}} \tag{4}$$

and $\mathbf{r}_{p_0}$ is the periapsis position vector of the initial parking orbit.

3) $0 < |\hat{\mathbf{h}}_0^\top \hat{\mathbf{v}}_\infty^+| < 1$ is the most general case. The departure orbit is neither normal nor coplanar to the parking orbit. In this case, $\hat{\mathbf{h}}_f$ is chosen to be the unit vector normal to $\hat{\mathbf{v}}_\infty^+$ that is closest to $\hat{\mathbf{h}}_0$, so that the angle between the initial parking orbit and departure orbit planes is minimized

$$\hat{\mathbf{h}}_f = \frac{\hat{\mathbf{v}}_\infty^+ \times (\hat{\mathbf{h}}_0 \times \hat{\mathbf{v}}_\infty^+)}{\|\hat{\mathbf{v}}_\infty^+ \times (\hat{\mathbf{h}}_0 \times \hat{\mathbf{v}}_\infty^+)\|} \tag{5}$$

It is noted that $\hat{\mathbf{h}}_f$ is always defined if $0 \le |\hat{\mathbf{h}}_0 \cdot \hat{\mathbf{v}}_\infty^+| < 1$. As constructed, $\hat{\mathbf{h}}_f$ is along the projection of $\hat{\mathbf{h}}_0$ onto the plane that is normal to $\hat{\mathbf{v}}_\infty^+$. The three vectors $\hat{\mathbf{v}}_\infty^+$, $\hat{\mathbf{h}}_0$, and $\hat{\mathbf{h}}_f$ are all in the same plane. Furthermore, this same expression can be used to get the $\hat{\mathbf{h}}_f$ vector for the case $|\hat{\mathbf{h}}_0 \cdot \hat{\mathbf{v}}_\infty^+| = 0$, which leads to the same result for $\hat{\mathbf{h}}_f$; indeed, the closest unit vector to $\hat{\mathbf{h}}_0$ that is normal to $\hat{\mathbf{v}}_\infty^+$ is $\hat{\mathbf{h}}_0$ itself, when $|\hat{\mathbf{h}}_0 \cdot \hat{\mathbf{v}}_\infty^+| = 0$.

A. One-Impulse TEI Transfer

Beginning with a parking orbit around the moon, the goal is to compute the single injection maneuver to achieve a specified outgoing hyperbolic excess velocity vector $\mathbf{v}_\infty^+$. The injection maneuver can be made at any point along the parking orbit. However, there is one location on the parking orbit that yields the best maneuver in terms of minimum Δv. First, to get an initial feasible estimate, an escape trajectory that minimizes the required plane change is assumed such that its angular momentum vector is closest to that of the initial parking orbit.

For labeling purposes, there are two orbits referred to as orbit 0 and orbit f. Orbit 0 is the initial parking orbit around the moon and orbit f is the postmaneuver hyperbolic orbit that contains the target $\mathbf{v}_\infty^+$. Orbit f is computed as follows. The injection maneuver is

$$\Delta\mathbf{v}_1 = \mathbf{v}_1^+ - \mathbf{v}_1^- \tag{6}$$

where $\mathbf{v}_1^+$ and $\mathbf{v}_1^-$ are to be determined along with the position vector, $\mathbf{r}_1$, at which the maneuver is applied, occurring at t_1 on the parking orbit. For example, a single impulse transfer targeting a $\mathbf{v}_\infty^+$ of relative declination 50° with respect to the parking orbit is shown in Fig. 1.

Having determined $\hat{\mathbf{h}}_f$, the remaining elements of the departure hyperbola can now be computed. The semimajor axis is known

$$a_f = -\frac{\mu_{\text{moon}}}{v_\infty^2} \tag{7}$$

where μ_{moon} is the gravitational parameter of the moon and $v_\infty = \|\mathbf{v}_\infty^+\|$. Unless otherwise specified, μ will be used in place of μ_{moon} in the equations that follow.

The position vector at which the departure maneuver is made $\mathbf{r}_1$ must lie both in the parking orbit's plane and in the escape orbit's plane. In this analysis, it depends on whether the planes of the parking and departure orbits simply intersect or fully coincide. Hence the subcases associated with those above with an additional qualifier regarding the eccentricity of the parking orbit are considered below:

1) $\hat{\mathbf{h}}_0 \cdot \hat{\mathbf{v}}_\infty^+ = 0$ (orbit planes are coincident, $\hat{\mathbf{h}}_0 \| \hat{\mathbf{h}}_f$) and $e_0 = 0$ (parking orbit is circular). This is the trivial case. $\mathbf{r}_1$ is the periapsis position vector of the departure hyperbola

$$\mathbf{r}_1 = r_0\hat{\mathbf{r}}_{p_f} \tag{8}$$

where r_0 is the radius of the circular parking orbit

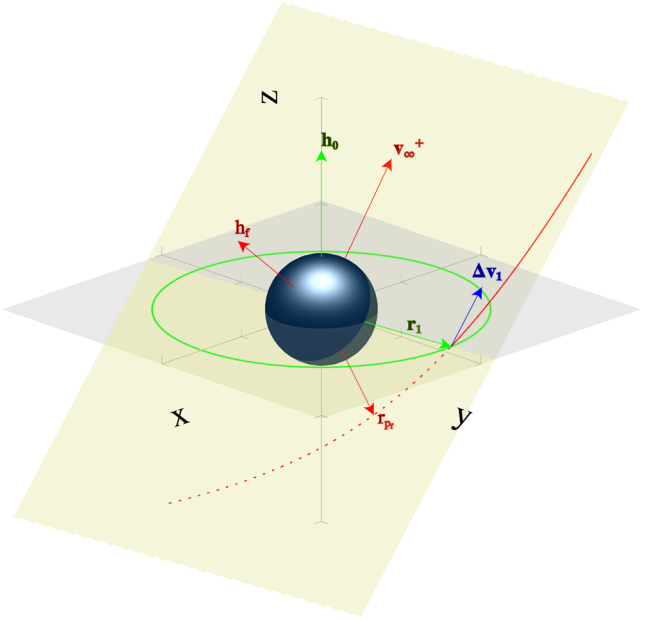

Fig. 1 Escape from the moon with a one-impulse TEI transfer targeting a $\mathbf{v}_\infty^+$ of relative declination 50°. The horizontal and inclined planes are, respectively, the parking orbit plane and the escape plane. The unique maneuver is performed at $\mathbf{r}_1$, and $\mathbf{v}_\infty^+$, $\mathbf{h}_0$, and $\mathbf{h}_f$ are in the same plane.

$$\hat{\mathbf{r}}_{p_f} = \frac{\hat{\mathbf{v}}_\infty^- - \hat{\mathbf{v}}_\infty^+}{\|\hat{\mathbf{v}}_\infty^- - \hat{\mathbf{v}}_\infty^+\|} \tag{9}$$

$$\hat{\mathbf{v}}_\infty^- = (\cos\delta)\hat{\mathbf{v}}_\infty^+ + (\sin\delta)(\hat{\mathbf{v}}_\infty^+ \times \hat{\mathbf{h}}_f) \tag{10}$$

$$\delta = 2\arcsin\frac{1}{e_f} \tag{11}$$

$$e_f = \sqrt{1 - \frac{h_f^2}{a_f \mu}} \tag{12}$$

$$h_f = r_{p_f} v_{p_f}^+ \tag{13}$$

$$v_{p_f}^+ = \sqrt{\mu\left(\frac{2}{r_{p_f}} - \frac{1}{a_f}\right)} \tag{14}$$

and the velocity vector at periapsis on the departure hyperbola is

$$\mathbf{v}_{p_f}^+ = v_{p_f}^+ \hat{\mathbf{v}}_{p_f} \tag{15}$$

$$\hat{\mathbf{v}}_{p_f} = \frac{\hat{\mathbf{v}}_\infty^- + \hat{\mathbf{v}}_\infty^+}{\|\hat{\mathbf{v}}_\infty^- + \hat{\mathbf{v}}_\infty^+\|} \tag{16}$$

The velocity vector before the departure maneuver is

$$\mathbf{v}_{p_f}^- = v_{p_f}^- \hat{\mathbf{v}}_{p_f} \tag{17}$$

where

$$v_{p_f}^- = \sqrt{\frac{\mu}{r_0}} \tag{18}$$

The maneuver is

$$\Delta\mathbf{v} = \mathbf{v}_{p_f}^+ - \mathbf{v}_{p_f}^- \tag{19}$$

and it is made at $\mathbf{r}_1$.

2) $\hat{\mathbf{h}}_0^\top \hat{\mathbf{v}}_\infty^+ = 0$ and $0 < e_0 < 1$ (orbit planes are coincident and parking orbit is elliptical), or $\hat{\mathbf{h}}_0^\top \hat{\mathbf{v}}_\infty^+ \neq 0$ and $0 \leq e_0 < 1$ (orbit planes intersect and parking orbit is circular or elliptical). This is the most general case. The direction of the position vector of the maneuver is given by

$$\hat{\mathbf{r}}_1 = \frac{\hat{\mathbf{v}}_\infty^+ \times \hat{\mathbf{h}}_f}{\|\hat{\mathbf{v}}_\infty^+ \times \hat{\mathbf{h}}_f\|} \tag{20}$$

The true anomaly of $\mathbf{r}_1$ on orbit 0 (the parking orbit) must be determined. It is referred to as ν_{1_o} and is the angle between $\hat{\mathbf{r}}_{p_0}$ (the periapsis direction vector of orbit 0) and $\hat{\mathbf{r}}_1$ that is measured positive about $\hat{\mathbf{h}}_0$ from $\hat{\mathbf{r}}_{p_0}$

$$\nu_{1_0} = \text{sign}(\hat{\mathbf{h}}_0 \cdot (\hat{\mathbf{r}}_{p_0} \times \hat{\mathbf{r}}_1))\arccos(\hat{\mathbf{r}}_{p_0} \cdot \hat{\mathbf{r}}_1) \tag{21}$$

It is noted that $-\pi \leq \nu_{1_0} \leq \pi$, which can then be modulated to be between 0 and 2π. The magnitude of $\mathbf{r}_1$ is

$$r_1 = \frac{p_0}{1 + e_0 \cos\nu_{1_0}} \tag{22}$$

where p_0 is the parameter of the parking orbit, so that

$$\mathbf{r}_1 = r_1 \hat{\mathbf{r}}_1 \tag{23}$$

The hyperbola that contains both $\mathbf{r}_1$ and $\mathbf{v}_\infty^+$ must be determined. It is observed that $\mathbf{r}_1$ is not necessarily the periapsis position vector of the departure hyperbola, and that it lies at the intersection of both orbit planes, between the periapsis vector of the hyperbola $\mathbf{r}_{p_f}$ and its outgoing asymptote. The true anomaly of $\mathbf{r}_1$ on the hyperbola ν_{1_f} is unknown and satisfies the polar equation

$$r_1 = \frac{a_f(1 - e_f^2)}{1 + e_f \cos\nu_{1_f}} \tag{24}$$

where the value of a_f is given by Eq. (7). The eccentricity of the departure hyperbola e_f is also unknown. With ν_∞^+ being the true anomaly associated with $\mathbf{v}_\infty^+$, it is known that $0 \leq \nu_{1_f} < \nu_\infty^+$. The angle between $\hat{\mathbf{r}}_1$ and $\hat{\mathbf{v}}_\infty^+$ is $\frac{\pi}{2}$, from Eq. (20). With

$$\nu_{1_f} + \frac{\pi}{2} = \nu_\infty^+ \tag{25}$$

and knowing that

$$\cos\nu_\infty^+ = -\frac{1}{e_f} \tag{26}$$

Equations (24) and (25) are combined to obtain the system of nonlinear equations

$$\begin{cases} r_1 & = \frac{a_f(1-e_f^2)}{1+e_f \sin\nu_\infty^+} \\ \cos\nu_\infty^+ & = -\frac{1}{e_f} \end{cases} \tag{27}$$

with unknowns e_f and ν_∞^+, and which has a unique solution in the ranges $1 < e_f < \infty$ and $\frac{\pi}{2} < \nu_\infty^+ < \pi$. The solution of this system is

$$e_f = \frac{\sqrt{1 + 2\kappa^2 + 2\kappa + \sqrt{1+4\kappa}}}{\sqrt{2}\kappa} \quad \text{where } \kappa = -\frac{a_f}{r_1} \tag{28a}$$

$$\nu_\infty^+ = \arccos\left(-\frac{1}{e_f}\right) \tag{28b}$$

The true anomaly on the hyperbola associated with $\mathbf{r}_1$ is found from Eq. (25)

$$\nu_{1_f} = \nu_\infty^+ - \frac{\pi}{2} \tag{29}$$

and the turning angle of the hyperbola is

$$\delta = 2\arcsin\frac{1}{e_f} \tag{30}$$

$\hat{\mathbf{v}}_\infty^-$, which is obtained from the turning angle δ, together with $\hat{\mathbf{v}}_\infty^+$, are both used to obtain $\hat{\mathbf{r}}_{p_f}$ and $\hat{\mathbf{v}}_{p_f}$ of the hyperbola. The incoming hyperbolic excess velocity vector $\hat{\mathbf{v}}_\infty^-$ is

$$\hat{\mathbf{v}}_\infty^- = (\cos\delta)\hat{\mathbf{v}}_\infty^+ + (\sin\delta)(\hat{\mathbf{v}}_\infty^+ \times \hat{\mathbf{h}}_f) \tag{31}$$

The direction of the periapsis position and velocity vectors of the hyperbola are

$$\hat{\mathbf{r}}_{p_f} = \frac{\hat{\mathbf{v}}_\infty^- - \hat{\mathbf{v}}_\infty^+}{\|\hat{\mathbf{v}}_\infty^- - \hat{\mathbf{v}}_\infty^+\|}, \qquad \hat{\mathbf{v}}_{p_f} = \frac{\hat{\mathbf{v}}_\infty^- + \hat{\mathbf{v}}_\infty^+}{\|\hat{\mathbf{v}}_\infty^- + \hat{\mathbf{v}}_\infty^+\|} \tag{32}$$

The periapsis position and velocity vectors of the hyperbola are

$$\mathbf{r}_{p_f} = r_{p_f}\hat{\mathbf{r}}_{p_f}, \qquad \mathbf{v}_{p_f} = v_{p_f}^+\hat{\mathbf{v}}_{p_f} \tag{33}$$

where

$$r_{p_f} = a_f(1-e_f), \qquad v_{p_f}^+ = \frac{h_f}{r_{p_f}} \quad \text{with} \quad h_f = \sqrt{\mu a_f(1-e_f^2)} \tag{34}$$

The postmaneuver velocity required at $\mathbf{r}_1$ is based on the parameterization of the velocity vector in the perifocal reference frame and uses the perapsis position and velocity unit vectors

$$\mathbf{v}_1^+ = \sqrt{\frac{\mu}{p_f}}[(-\sin\nu_{1_f})\hat{\mathbf{r}}_{p_f} + (e_f + \cos\nu_{1_f})\hat{\mathbf{v}}_{p_f}] \tag{35}$$

The same holds for the premaneuver velocity on orbit 0

$$\mathbf{v}_1^- = \sqrt{\frac{\mu}{p_0}}[(-\sin\nu_{1_0})\hat{\mathbf{r}}_{p_0} + (e_0 + \cos\nu_{1_0})\hat{\mathbf{v}}_{p_0}] \tag{36}$$

Finally, the required maneuver is

$$\Delta\mathbf{v}_1 = \mathbf{v}_1^+ - \mathbf{v}_1^- \tag{37}$$

This completes the construction of the one-maneuver TEI sequence.

3) When a plane change is required and the eccentricity of the parking orbit is relatively small, the initial estimate for the TEI-1 maneuver can be further improved in terms of Δv by choosing an adequate direction of the angular momentum of the escape hyperbola $\hat{\mathbf{h}}_f$, different from that obtained from Eq. (5). Knowing that $\hat{\mathbf{h}}_f$ must be orthogonal to $\mathbf{v}_\infty^+$, which is fixed, the former can be rotated about the latter by increments of 1 deg to perform a scanning and finally retain the direction of $\hat{\mathbf{h}}_f$ that leads to the smallest magnitude of the maneuver $\Delta\mathbf{v}_1$. With $\hat{\mathbf{h}}_f^\star$ representing the new direction of the angular momentum vector, and Θ the angle between $\hat{\mathbf{h}}_f^\star$ and the plane defined by the vectors $\hat{\mathbf{h}}_0$ and $\hat{\mathbf{v}}_\infty^+$, it can be calculated by

$$\hat{\mathbf{h}}_f^\star = \mathcal{R}(\hat{\mathbf{v}}_\infty^+, \Theta)\hat{\mathbf{h}}_f \tag{38}$$

where $\mathcal{R}(\Gamma, \xi)$ is a matrix representing the rotation of an angle ξ about the normalized axis Γ of coordinates (x, y, z); the expression for $\mathcal{R}$ is

$$\mathcal{R}(\Gamma(x,y,z),\xi) = \begin{pmatrix} x^2(1-c)+c & xy(1-c)-zs & xz(1-c)+ys \\ yx(1-c)+zs & y^2(1-c)+c & yz(1-c)-xs \\ xz(1-c)-ys & yz(1-c)+xs & z^2(1-c)+c \end{pmatrix} \tag{39}$$

where $c = \cos\xi$ and $s = \sin\xi$, and $\|\Gamma\|^2 = x^2 + y^2 + z^2 = 1$.

The maneuver has to be performed at the intersection line of the parking and escape orbit planes, i.e., on the line that is at the intersection of the planes with normal vectors are $\hat{\mathbf{h}}_0$ and $\hat{\mathbf{h}}_f^\star$. Thus, the new position of the maneuver $\Delta\mathbf{v}_1$ is

$$\hat{\mathbf{r}}_1 = \text{sign}(\hat{\mathbf{h}}_0 \cdot \hat{\mathbf{v}}_\infty^+)\frac{\hat{\mathbf{h}}_0 \times \hat{\mathbf{h}}_f^\star}{\|\hat{\mathbf{h}}_0 \times \hat{\mathbf{h}}_f^\star\|} \tag{40}$$

The true anomaly of the maneuver on the parking orbit ν_{1_0} is calculated from Eq. (21). It is noted that $-\pi \le \nu_{1_O} \le \pi$, which can then be modulated to be between 0 and 2π. Using Eq. (23), the position vector of the maneuver, $\mathbf{r}_1$, is obtained, whose magnitude is calculated from Eq. (22).

Examination of the escape orbit plane shows that the angle between $\hat{\mathbf{r}}_1$ and $\hat{\mathbf{v}}_\infty^+$ is defined by

$$\Delta\nu = \nu_\infty^+ - \nu_{1_f} \tag{41}$$

and can be calculated from

$$\Delta\nu = \arccos(\hat{\mathbf{r}}_1 \cdot \hat{\mathbf{v}}_\infty^+) \tag{42}$$

Combining Eqs. (24), (26), and (41), the following system of nonlinear equations is obtained

$$\begin{cases} r_1 = \dfrac{a_f(1-e_f^2)}{1 + e_f\cos\nu_{1_f}} \\ \cos\nu_{1_f} = -\dfrac{1}{e_f}\cos\Delta\nu + \dfrac{\sqrt{e_f^2-1}}{e_f}\sin\Delta\nu \end{cases} \tag{43}$$

with unknowns e_f and ν_{1_f}, and which has a unique solution in the ranges $1 < e_f < \infty$ and $0 < \nu_{1_f} < \pi$. The solution of this system is

$$e_f = \frac{\sqrt{\sin^2\Delta\nu + 2\kappa^2 + 2\kappa(1-\cos\Delta\nu) + \sin\Delta\nu\sqrt{\sin^2\Delta\nu + 4\kappa(1-\cos\Delta\nu)}}}{\sqrt{2}\kappa} \tag{44a}$$

$$\nu_{1_f} = \arccos\left(-\frac{1}{e_f}\cos\Delta\nu + \frac{\sqrt{e_f^2-1}}{e_f}\sin\Delta\nu\right) \tag{44b}$$

where κ is defined in Eq. (28a). Steps from Eq. (30) through Eq. (37) are repeated.

B. Three-Impulse TEI Transfer

As was done for the one-impulse TEI transfer, the goal of the three-impulse transfer sequence is to achieve the asymptotic velocity vector $\mathbf{v}_\infty^+$ from a closed parking orbit around the moon. Furthermore, the departure orbit plane is assumed to be not coincident with that of the parking orbit ($\hat{\mathbf{h}}_0 \cdot \hat{\mathbf{v}}_\infty \neq 0$), meaning that a plane change is required. In the case that the orbit planes are coincident, the single TEI maneuver discussed previously is used, as a one-impulse maneuver will be optimum in this particular case [1].

The first maneuver is an in-plane maneuver that raises apoapsis, which is bounded from above. The second maneuver occurs at

apoapsis of the premaneuver orbit. This maneuver is considered as the plane change maneuver but it can also affect the magnitude of the periapsis radius of the post maneuver orbit. This periapsis point is bound from below. The third maneuver is an in-plane maneuver that occurs at periapsis and produces the needed escape orbit that contains the target $\mathbf{v}_\infty^+$ vector. In the construction of the three-impulse initial estimate, all maneuvers are assumed to occur at the apsides of the corresponding premaneuver orbits; however, this does not imply that the flight-path angle after a maneuver is necessarily zero.

For labeling purposes there are four orbits referred to as orbit 0–orbit 3; as before, orbit 0 is the parking orbit and orbits 1, 2, and 3 are described as follows:

1) Orbit 1 is an elliptical orbit, with periapsis radius r_{p_1} and apoapsis radius r_{a_1}, which is achieved after $\Delta\mathbf{v}_1$ and is in the same plane as orbit 0; r_{a_1} is specified and is typically in the range $10,000 \lesssim r_{a_1} \lesssim 17,000$ km. The reason for this range is due to practical considerations. The apoapsis radius of orbit 1 is such that the time period of this orbit is on the order of a day or two; r_{p_1} needs to be determined because it lies somewhere on the parking orbit, which can be elliptical. $\Delta\mathbf{v}_1$ is a pure apoapsis raising maneuver that occurs at $\mathbf{r}_{p_1}$

$$\Delta\mathbf{v}_1 = \mathbf{v}_{p_1}^+ - \mathbf{v}_{p_1}^- \tag{45}$$

$\mathbf{r}_{p_1}, \mathbf{v}_{p_1}^+, \mathbf{v}_{p_1}^-$ are to be determined.

2) Orbit 2 is an orbit that is in the same plane as the departure hyperbola, which is orbit 3. In the construction of this initial estimate, it is possible that orbit 2 is closed or open; i.e., its eccentricity is strictly positive. The periapsis radius of orbit 2 is required to be no less than a specified amount, typically the periapsis radius of orbit 0, $r_{p_2} \geq r_{p_0}$. $\Delta\mathbf{v}_2$ is generally a plane change maneuver but it can also raise (or lower) the periapsis radius of the premaneuver orbit. The maneuver occurs at the apoapsis of orbit 1, which is not necessarily the same as the apoapsis point of orbit 2, if orbit 2 is an ellipse. This is because the line of apsides of orbit 2 is not necessarily in the plane of orbit 1. The line of apsides of orbit 2 is aligned with the line of apsides of the departure orbit, orbit 3, and this line is generally out of the plane of Orbits 0 and 1. $\Delta\mathbf{v}_2$ occurs at $\mathbf{r}_{a_1}$, which is determined by the procedure to be described, and is defined by

$$\Delta\mathbf{v}_2 = \mathbf{v}_2^+ - \mathbf{v}_2^- \tag{45}$$

where $\mathbf{v}_2^- = \mathbf{v}_{a_1}$ is the velocity at apoapsis of orbit 1. So, $\mathbf{r}_{a_1}, \mathbf{v}_2^+, \mathbf{v}_{a_1}$ are to be determined.

3) Orbit 3 is the departure hyperbola and is in the same plane as orbit 2. It is produced by the maneuver $\Delta\mathbf{v}_3$, which occurs at the periapsis point of orbit 3, which is the same as the periapsis point of orbit 2. $\Delta\mathbf{v}_3$ occurs along the velocity vector at $\mathbf{r}_{p_3}$ and is the escape maneuver that achieves the necessary hyperbolic excess velocity vector $\mathbf{v}_\infty^+$

$$\Delta\mathbf{v}_3 = \mathbf{v}_{p_3}^+ - \mathbf{v}_{p_3}^- \tag{46}$$

$\mathbf{r}_{p_3}, \mathbf{v}_{p_3}^+, \mathbf{v}_{p_3}^-$ are to be determined.

A graph of a three-impulse transfer targeting a $\mathbf{v}_\infty^+$ of relative declination 60° with respect to the parking orbit is shown in Fig. 2.

Again, the parking orbit around the moon is defined in a fixed moon-centered frame and $\mathbf{v}_\infty^+$ is referred to this reference frame. The unit vector normal to the departure orbit plane $\hat{\mathbf{h}}_f$ is computed as described above in Eq. (5). The angular momentum direction of orbit 3 $\hat{\mathbf{h}}_3$ is

$$\hat{\mathbf{h}}_3 = \hat{\mathbf{h}}_f \tag{47}$$

The remaining elements of this hyperbola need to be computed and it is assumed that its periapsis radius is known, $r_{p_3} = r_{p_2}$, which is specified, but is required to be greater than the periselene of the parking orbit, r_{p_0} ($r_{p_3} \geq r_{p_0}$). The semimajor axis of the hyperbola is

$$a_3 = \frac{-\mu}{v_\infty^2} \tag{48}$$

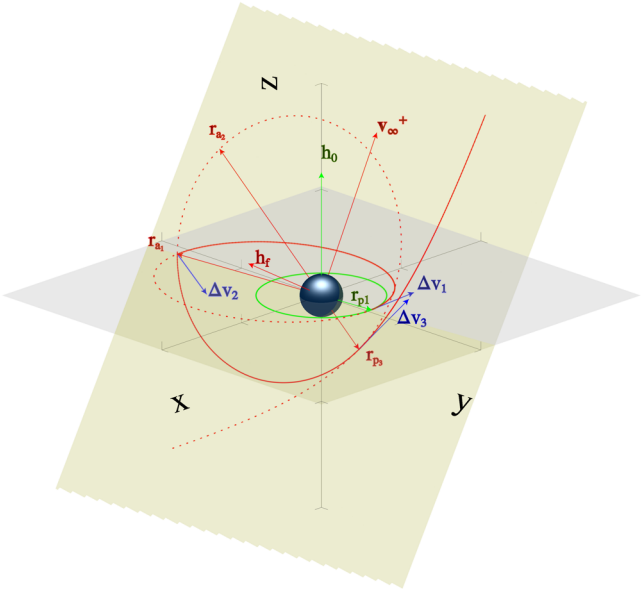

Fig. 2 Escape from the moon with a three-impulse TEI transfer targeting a $\mathbf{v}_\infty^+$ of relative declination 60°. The horizontal and inclined planes are, respectively, the parking orbit plane and the escape plane. The first maneuver is performed at $\mathbf{r}_{p_1}$, the second one at $\mathbf{r}_{a_1}$, and the third one at $\mathbf{r}_{p_3}$. Orbits 0 and 1 are in the same plane, as well as orbits 2 and 3, respectively.

which is negative. The periapsis velocity at r_{p_3} is

$$v_{p_3}^+ = \sqrt{v_\infty^2 + \frac{2\mu}{r_{p_3}}} \tag{49}$$

and the magnitude of the hyperbola's angular momentum vector is

$$h_3 = r_{p_3} v_{p_3}^+ \tag{50}$$

The angular momentum vector of orbit 3 is

$$\mathbf{h}_3 = h_3 \hat{\mathbf{h}}_3 \tag{51}$$

The periapsis radius and velocity vectors $\mathbf{r}_{p_3}$ and $\mathbf{v}_{p_3}^+$ are now computed; $\mathbf{v}_{p_3}^+$ is the resulting velocity vector after $\Delta\mathbf{v}_3$. To find $\hat{\mathbf{v}}_\infty^-$, knowing that $\hat{\mathbf{v}}_\infty^+$ and $\hat{\mathbf{v}}_\infty^-$ are both in the plane that is orthogonal to $\hat{\mathbf{h}}_3$, $\hat{\mathbf{v}}_\infty^+$ is rotated clockwise about $\hat{\mathbf{h}}_3$ (looking down on $\hat{\mathbf{h}}_3$) through the turning angle of the hyperbola which is δ. The eccentricity of orbit 3 is

$$e_3 = \sqrt{1 - \frac{h_3^2}{a_3 \mu}} \tag{52}$$

and the turning angle δ of the hyperbola is found from Eq. (30) (as $e_3 = e_f$). $\hat{\mathbf{v}}_\infty^-$ is given by Eq. (31). As orbit 3 and orbit f are equivalent in this case, the periapsis position and velocity vectors of the departure hyperbola are obtained from Eqs. (32) and (33) ($\mathbf{r}_{p_3} = \mathbf{r}_{p_f}$ and $\mathbf{v}_{p_3} = \mathbf{v}_{p_f}$). Orbit 3 is now completely defined. To obtain $\mathbf{v}_{p_3}^-$, knowledge of the elements of orbit 2 is required. The line of apsides for orbit 2 is defined by aligning $\hat{\mathbf{r}}_{p_2}$ with $\hat{\mathbf{r}}_{p_3}$ so that

$$\hat{\mathbf{r}}_{p_2} = \hat{\mathbf{r}}_{p_3} \qquad \hat{\mathbf{r}}_{a_2} = -\hat{\mathbf{r}}_{p_2} \tag{53}$$

With this, the departure maneuver $\Delta\mathbf{v}_3$ will be in the velocity direction. However, the plane change and periapsis raising maneuvers will not occur at the apsides of orbit 2. Specifically, $\Delta\mathbf{v}_2$ occurs at $\mathbf{r}_{a_1}$, the intersection of the planes of orbit 1 and orbit 2. Recall that $r_{p_3} = r_{p_2}$ and r_{p_2} is specified. It is noted, in general, that $\hat{\mathbf{r}}_{p_3}$ is not in the orbit plane of the initial orbit. With this, it can also be stated that the line of apsides of orbit 2 is not in the plane of the initial parking orbit, but is contained in the plane of the departure orbit. In any case,

the planes of orbit 0 and orbit 1 coincide, as well as those of orbit 2 and orbit 3. The radius vector at which the second maneuver $\Delta\mathbf{v}_2$ is made to transition onto orbit 2 lies along the intersection of the planes of orbit 0 and orbit 3 and points away from $\hat{\mathbf{r}}_{p_3}$. This vector is named $\mathbf{r}_{a_1}$ because it will be the apoapsis radius vector of orbit 1. Its direction is

$$\hat{\mathbf{r}}_{a_1} = \frac{[\hat{\mathbf{r}}_{a_2} \times (\hat{\mathbf{h}}_3 \times \hat{\mathbf{h}}_0)] \times \hat{\mathbf{h}}_0}{\|[\hat{\mathbf{r}}_{a_2} \times (\hat{\mathbf{h}}_3 \times \hat{\mathbf{h}}_0)] \times \hat{\mathbf{h}}_0\|} = \frac{(\hat{\mathbf{h}}_0 \cdot \hat{\mathbf{r}}_{a_2})(\hat{\mathbf{h}}_3 \times \hat{\mathbf{h}}_0)}{\|(\hat{\mathbf{h}}_0 \cdot \hat{\mathbf{r}}_{a_2})(\hat{\mathbf{h}}_3 \times \hat{\mathbf{h}}_0)\|} \tag{54}$$

This vector is in the plane of all orbits (orbit 0 to orbit 3), and points away from $\hat{\mathbf{r}}_{p_2}$ (as well as $\hat{\mathbf{r}}_{p_3}$). It is noted that $\hat{\mathbf{r}}_{a_1}$ is not necessarily collinear with $\hat{\mathbf{r}}_{p_2}$ or $\hat{\mathbf{r}}_{p_3}$. If $\hat{\mathbf{h}}_3 \times \hat{\mathbf{h}}_0 = \mathbf{0}$, meaning that the parking orbit and the departure orbit are in the same plane, then let $\hat{\mathbf{r}}_{a_1} = \hat{\mathbf{r}}_{a_2}$. However, this particular case would be equivalent to a one-impulse TEI transfer in terms of Δv but would have a longer time of flight; so by default, a one-impulse transfer is used. The direction of periapsis of orbit 1 is now known; this fixes the direction of the location of the first maneuver $\Delta\mathbf{v}_1$ that makes the transition from orbit 0 (the parking orbit) to orbit 1

$$\hat{\mathbf{r}}_{p_1} = -\hat{\mathbf{r}}_{a_1} \tag{55}$$

To compute the position vector $\mathbf{r}_{p_1}$ of the maneuver $\Delta\mathbf{v}_1$, its magnitude r_{p_1} must be found: $\mathbf{r}_{p_1}$ is required to lie on orbit 0; let $\hat{\mathbf{r}}_{p_0}$ be the periapsis radius unit vector on orbit 0. The angle between $\hat{\mathbf{r}}_{p_0}$ and $\hat{\mathbf{r}}_{p_1}$ is measured positive about $\hat{\mathbf{h}}_0$ from $\hat{\mathbf{r}}_{p_0}$; it is the true anomaly associated with $\hat{\mathbf{r}}_{p_1}$ on orbit 0

$$\nu_{1_0} = \text{sign}(\hat{\mathbf{h}}_0 \cdot (\hat{\mathbf{r}}_{p_0} \times \hat{\mathbf{r}}_{p_1})) \arccos(\hat{\mathbf{r}}_{p_0} \cdot \hat{\mathbf{r}}_{p_1}) \tag{56}$$

ν_{1_0} is used to represent the true anomaly of $\hat{\mathbf{r}}_{p_1}$ on orbit 0. It is noted that $-\pi \leq \nu_{1_0} \leq \pi$ so that ν_{1_0} can be modulated to be between 0 and 2π. The magnitude of $\mathbf{r}_{p_1}$ is

$$r_{p_1} = \frac{p_0}{1 + e_0 \cos \nu_{1_0}} \tag{57}$$

so that

$$\mathbf{r}_{p_1} = r_{p_1} \hat{\mathbf{r}}_{p_1} \tag{58}$$

The periapsis and apoapsis velocity directions for orbit 1 are

$$\hat{\mathbf{v}}_{p_1} = \hat{\mathbf{h}}_1 \times \hat{\mathbf{r}}_{p_1} \qquad \hat{\mathbf{v}}_{a_1} = \hat{\mathbf{h}}_1 \times \hat{\mathbf{r}}_{a_1} \tag{59}$$

r_{a_1} being specified, the apoapsis radius vector of orbit 1 is

$$\mathbf{r}_{a_1} = r_{a_1} \hat{\mathbf{r}}_{a_1} \tag{60}$$

The elements of orbit 2 are required to determine the actual velocity after $\Delta\mathbf{v}_2$. The apoapsis radius vector of orbit 1 also lies somewhere after apoapsis on orbit 2. Indeed, along orbit 2, the apoapsis of orbit 1 is located after the apoapsis of orbit 2, as $\hat{\mathbf{r}}_{a_2} \times \hat{\mathbf{r}}_{a_1} = (\hat{\mathbf{r}}_{a_2} \cdot \hat{\mathbf{h}}_0)^2 \hat{\mathbf{h}}_3$. Thus, on orbit 2, the true anomaly of $\mathbf{r}_{a_1}$ is equal to $\pi + \Delta\nu$, where $\Delta\nu$ is defined as the angle between $\hat{\mathbf{r}}_{a_2}$ and $\hat{\mathbf{r}}_{a_1}$ measured positively about $\hat{\mathbf{h}}_3$ from $\hat{\mathbf{r}}_{a_2}$, such that

$$\Delta\nu = \arccos(\hat{\mathbf{r}}_{a_2} \cdot \hat{\mathbf{r}}_{a_1}) \tag{61}$$

The polar equation of a conic section for r_{a_1} must then be verified

$$r_{a_1} = \frac{a_2(1 - e_2^2)}{1 + e_2 \cos(\pi + \Delta\nu)} \tag{62}$$

With $r_{p_2} = a_2(1 - e_2)$ and solving for a_2

$$a_2 = \frac{r_{p_2}}{1 - e_2} \tag{63}$$

This is inserted into Eq. (64) to obtain e_2

$$e^2 = \frac{r_{a_1} - r_{p_2}}{r_{a_1} \cos(\Delta\nu) + r_{p_2}} \tag{64}$$

With Eq. (64), a_2 is determined from Eq. (63). It is noted that orbit 2 does not need to be an ellipse because for a small enough r_{p_2}, orbit 2 can be hyperbolic. With this, orbits 1 and 2 are now completely defined.

The velocity on orbit 2 at $\mathbf{r}_{a_1}$ is $\mathbf{v}_2^+$ which denotes that it is the velocity required after the second maneuver $\Delta\mathbf{v}_2$; it is

$$\mathbf{v}_2^+ = \sqrt{\frac{\mu}{a_2(1 - e_2^2)}}[(-\sin(\pi + \Delta\nu))\hat{\mathbf{r}}_{p_2} + (e_2 + \cos(\pi + \Delta\nu))\hat{\mathbf{v}}_{p_2}] \tag{65}$$

where

$$\hat{\mathbf{v}}_{p_2} = \hat{\mathbf{h}}_2 \times \hat{\mathbf{r}}_{p_2} \tag{66}$$

It is understood that the second maneuver does not necessarily occur at the apoapsis point of orbit 2, but it does occur at the apoapsis point of orbit 1. The velocity right before $\Delta\mathbf{v}_2$ is $\mathbf{v}_{a_1}^-$ and is computed as follows:

$$a_1 = \frac{r_{p_1} + r_{a_1}}{2} \tag{67}$$

$$v_{a_1} = \sqrt{\mu\left(\frac{2}{r_{a_1}} - \frac{1}{a_1}\right)} \tag{68}$$

$$\hat{\mathbf{v}}_{a_1} = \hat{\mathbf{h}}_1 \times \hat{\mathbf{r}}_{a_1} \tag{69}$$

$$\mathbf{v}_{a_1} = v_{a_1} \hat{\mathbf{v}}_{a_1} \tag{70}$$

Let

$$\mathbf{v}_2^- = \mathbf{v}_{a_1} \tag{71}$$

So finally

$$\Delta\mathbf{v}_2 = \mathbf{v}_2^+ - \mathbf{v}_2^- \tag{72}$$

Regarding the first maneuver $\Delta\mathbf{v}_1$, the velocity at periapsis of orbit 1 is computed from

$$v_{p_1} = \sqrt{\mu\left(\frac{2}{r_{p_1}} - \frac{1}{a_1}\right)} \tag{73}$$

so that

$$\mathbf{v}_{p_1} = v_{p_1} \hat{\mathbf{v}}_{p_1} \tag{74}$$

Let

$$\mathbf{v}_1^+ = \mathbf{v}_{p_1} \tag{75}$$

and

$$\mathbf{v}_1^- = \sqrt{\frac{\mu}{p_0}}[(-\sin \nu_{1_O})\hat{\mathbf{r}}_{p_0} + (e_0 + \cos \nu_{1_O})\hat{\mathbf{v}}_{p_0}] \tag{76}$$

So finally

$$\Delta\mathbf{v}_1 = \mathbf{v}_1^+ - \mathbf{v}_1^- \tag{77}$$

Regarding the third maneuver $\Delta\mathbf{v}_3$, the velocity at periapsis of orbit 2 is computed from

$$v_{p_2} = \sqrt{\mu\left(\frac{2}{r_{p_2}} - \frac{1}{a_2}\right)} \tag{78}$$

so that

$$\mathbf{v}_{p_2} = v_{p_2}\hat{\mathbf{v}}_{p_2} \quad \text{with} \quad \hat{\mathbf{v}}_{p_2} = \hat{\mathbf{v}}_{p_3} \tag{79}$$

Let

$$\mathbf{v}_3^+ = \mathbf{v}_{p3} \quad \text{and} \quad \mathbf{v}_3^- = \mathbf{v}_{p_2} \tag{80}$$

So finally

$$\Delta\mathbf{v}_3 = \mathbf{v}_3^+ - \mathbf{v}_3^- \tag{81}$$

This procedure yields the estimate of the three-maneuver TEI transfer sequence.

V. Initial Estimate for the Complete Moon-to-Earth Trajectory

The procedure for constructing the initial estimate of the complete moon-to-Earth impulsive trajectory is outlined below. The information that is given is:

1. t_m, $\mathbf{r}_m$, $\mathbf{v}_m$: epoch and state of the initial moon-centered orbit.

2. $r(t_e)$, $\phi(t_e)$: the desired radius and latitude associated with the Earth entry interface point in an Earth fixed frame. It is noted that the other flight coordinates, such as the flight-path angle at EEI, can also be specified and targeted.

The following quantities must be estimated:

1) From the moon: the times at which the maneuvers are performed, as well as their $\Delta\mathbf{v}$ vectors, and the time of flight from the epoch t_m to the moon's sphere of influence.

2) From the Earth: the state of the spacecraft ($\mathbf{r}_{t_e}$, $\mathbf{v}_{t_e}$) and time t_e at EEI, as well as the time of flight (backward in time) from EEI to the moon's sphere of influence.

The time at which the spacecraft reaches the moon's sphere of influence is t_{soi}. The steps to generate the initial estimate are:

1) The antipode state at the Earth associated with the moon's position at t_m is constructed. The position vector of the moon is obtained in an ECI (Earth-centered inertial) frame at t_m, $\mathbf{r}_{\text{moon}}(t_m)$, and is used as the line of apsides for an Earth–moon backward Hohmann transfer.

2) This antipode state is $[\mathbf{r}(t_e), \mathbf{v}(t_e)]$ and the direction of perigee of the Hohmann transfer ellipse at t_e is

$$\hat{\mathbf{r}}_p(t_e) = -\frac{\mathbf{r}_{\text{moon}}(t_m)}{r_{\text{moon}}(t_m)} \tag{82}$$

The unit vector $\hat{\mathbf{r}}_p(t_e)$ is parameterized with a declination δ and a right ascension α

$$\hat{\mathbf{r}}_p(t_e) = \begin{pmatrix} \cos\delta\cos\alpha \\ \cos\delta\sin\alpha \\ \sin\delta \end{pmatrix} \tag{83}$$

This is the moon's antipode vector. The right ascension and declination of $\hat{\mathbf{r}}_p(t_e)$ are obtained by transforming its components from Cartesian to spherical coordinates.

3. Because $-\frac{\pi}{2} \le \delta \le +\frac{\pi}{2}$, then:

a) If $\phi(t_e) \ge \delta$, it is an incoming (in forward time) North Pole flyby and the angular momentum vector direction of the incoming state at t_e is chosen to be

$$\hat{\mathbf{h}}_{t_e} = \frac{\hat{\mathbf{k}} \times \hat{\mathbf{r}}_p(t_e)}{\|\hat{\mathbf{k}} \times \hat{\mathbf{r}}_p(t_e)\|} \tag{84}$$

and the incoming azimuth is

$$\gamma_{\text{eci}} = \pi \tag{85}$$

b) If $\phi(t_e) < \delta$, it is an incoming South Pole flyby and the angular momentum vector of the trajectory is chosen to be

$$\hat{\mathbf{h}}_{t_e} = \frac{\hat{\mathbf{r}}_p(t_e) \times \hat{\mathbf{k}}}{\|\hat{\mathbf{r}}_p(t_e) \times \hat{\mathbf{k}}\|} \tag{86}$$

and the incoming azimuth is

$$\gamma_{\text{eci}} = 0 \tag{87}$$

where $\hat{\mathbf{k}}$ is the unit vector normal to the equatorial plane of the ECI reference frame.

4) In either case, the true anomaly at t_e of the incoming trajectory is

$$\nu_{\text{te}} = -|\phi - \delta| \tag{88}$$

The direction of the incoming periapsis velocity vector is

$$\hat{\mathbf{v}}_{p_{\text{te}}} = \hat{\mathbf{h}}_{\text{te}} \times \hat{\mathbf{r}}_{p_{\text{te}}} \tag{89}$$

5) A backward time Hohmann transfer ellipse is constructed. Given r_{te} and knowing ν_{te}, the semimajor axis and eccentricity of the Hohmann transfer ellipse, a_{ht} and e_{ht} respectively, can be found. Knowing that the radius at apogee is $r_a = r_{\text{moon}}$ and that $r_a = a_{\text{ht}}(1 + e_{\text{ht}})$, use

$$r(t_e) = \frac{r_a(1 - e_{\text{ht}})}{1 + e_{\text{ht}}\cos\nu(t_e)} \tag{90}$$

to obtain e_{ht},

$$e_{\text{ht}} = \frac{r_a - r_{\text{te}}}{(r_{\text{te}}\cos\nu_{\text{te}} + r_a)} \tag{91}$$

and get a_{ht} from

$$a_{\text{ht}} = \frac{r_a}{1 + e_{\text{ht}}} \tag{92}$$

The periapsis radius of the incoming trajectory is then

$$r_{p_{\text{te}}} = a_{\text{ht}}(1 - e_{\text{ht}}) \tag{93}$$

It is noted that the spacecraft enters at a radius vector that is $r(t_e) \ge r_{p_{\text{te}}}$.

6) The backward transfer time on the ellipse is from ν_{te} to $\nu_f = \pi$ and is Δt. This is the same as the forward transfer time from $\nu_f = \pi$ to ν_{te}. The spacecraft is moving on the lower half plane of the arrival ellipse and Kepler's equation is used to get a first estimate of this travel time, which is known to be less than or equal to the half period of the Hohmann transfer ellipse

$$\Delta t \le \frac{T_p}{2} \tag{94}$$

where

$$T_p = 2\pi\sqrt{\frac{a_{\text{ht}}^3}{\mu_{\text{earth}}}} \tag{95}$$

so

$$t_e = t_m + \Delta t \tag{96}$$

This is the estimate for the epoch at the Earth entry interface point.

7) Calculate the state at the Earth entry interface $\mathbf{r}_{\text{te}}$, $\mathbf{v}_{\text{te}}$

$$\mathbf{r}_{t_e} = r_{t_e}[(\cos\nu_{\text{te}})\hat{\mathbf{r}}_{p_{\text{te}}} + (\sin\nu_{\text{te}})\hat{\mathbf{v}}_{p_{\text{te}}}] \tag{97}$$

$$\mathbf{v}_{t_e} = \sqrt{\frac{\mu_{\text{earth}}}{a_{\text{ht}}(1 - e_{\text{ht}}^2)}}[(-\sin\nu_{\text{te}})\hat{\mathbf{r}}_{p_{\text{te}}} + (e_{\text{ht}} + \cos\nu_{\text{te}})\hat{\mathbf{v}}_{p_{\text{te}}}] \tag{98}$$

8) Define the radius of an approximate sphere of influence about the moon

$$R_{\mathrm{soi}_M} \simeq 50,000 \text{ km} \tag{99}$$

where any number in the vicinity of the distance between the moon and the interior libration point of the Earth–moon system is suitable. The value of the true anomaly on the ellipse when the spacecraft reaches the moon's sphere of influence from the backward propagated Earth trajectory is approximated and this radial distance from the Earth is r_{soi}. It is known that

$$R_{\mathrm{soi}_M} + r_{\mathrm{soi}} \approx 2a_{\mathrm{ht}} \tag{100}$$

so r_{soi} can be estimated and is set to

$$r_{\mathrm{soi}} = 2a_{\mathrm{ht}} - R_{\mathrm{soi}_M} \tag{101}$$

This can be said because the distance from the vacant focus to the moon is small compared with the distance from the Earth to the moon; it is equal to $r_{p_{\mathrm{te}}}$. The true anomaly when the backward propagated Hohmann transfer ellipse reaches the moon's sphere of influence is

$$\nu_{\mathrm{soi}} = -\arccos\left[\frac{1}{e_{\mathrm{ht}}}\left(\frac{a_{\mathrm{ht}}(1-e_{\mathrm{ht}}^2)}{r_{\mathrm{soi}}} - 1\right)\right] \tag{102}$$

From this, the time of flight from ν_{te} to ν_{soi}, $t_{\mathrm{soi}} - t_e$, is estimated using Kepler's equation.

9) On the ellipse, the velocity vector at apoapsis $\mathbf{v}_a$ is computed. Knowing $\mathbf{v}_{\mathrm{moon}}(t_m)$, an estimate of the outgoing hyperbolic velocity excess vector at t_m is

$$\mathbf{v}_\infty^+ = \mathbf{v}_a - \mathbf{v}_{\mathrm{moon}}(t_m) \tag{103}$$

10) With the given t_m and the target $\mathbf{v}_\infty^+$, the procedure developed previously to construct feasible one and three-impulse escape sequences is used to compute a better estimate of t_{soi}. This is done because the duration of the escape sequence is nonzero as it has been assumed until now

$$t_{\mathrm{soi}} = t_m + \Delta t_{\mathrm{escape}} \tag{104}$$

where $\Delta t_{\mathrm{escape}}$ is the actual time from t_m to the point on the escape hyperbola from the moon when the spacecraft reaches the moon's sphere of influence; it is the time at which the spacecraft has almost reached $\mathbf{v}_\infty^+$. Also, the departure time t_{depart} is defined to be the time of the last maneuver at the moon that places the spacecraft on the departure hyperbola.

11) Knowing t_{depart}, the antipode state at the Earth at t_e is recomputed.

12) If the spacecraft needs to arrive at a specific target longitude in an Earth body fixed frame, then t_e is readjusted by plus or minus $\Delta\tau$, where $|\Delta\tau| \leq 12$ hours, so that the arrival state $\mathbf{r}(t_e)$, $\mathbf{v}(t_e)$ occurs at this target longitude.

13) Now, all the information to forward propagate the moon-centered state from t_m to t_{soi} using the one- or three-impulse escape sequence and to backward propagate the Earth-centered state from t_e to t_{soi} is available. The variable t_{soi} is allowed to have two values, one from the moon and one from the Earth, which are constrained to be equal at the end of the targeting procedure. There will be a position, velocity, and time mismatch near the patch point. These error deviations are

$$\Delta\mathbf{r}_{\mathrm{soi}} = \mathbf{r}_{\mathrm{earth}\to t\mathrm{soi}}(t_{\mathrm{soi}_{\mathrm{from}}\mathrm{earth}}) - \mathbf{r}_{\mathrm{moon}\to t\mathrm{soi}}(t_{\mathrm{soi}_{\mathrm{from}}\mathrm{moon}}) \tag{105}$$

$$\Delta\mathbf{v}_{\mathrm{soi}} = \mathbf{v}_{\mathrm{earth}\to t\mathrm{soi}}(t_{\mathrm{soi}_{\mathrm{from}}\mathrm{earth}}) - \mathbf{v}_{\mathrm{moon}\to t\mathrm{soi}}(t_{\mathrm{soi}_{\mathrm{from}}\mathrm{moon}}) \tag{106}$$

$$\Delta\mathbf{t}_{\mathrm{soi}} = t_{\mathrm{soi}_{\mathrm{from}}\mathrm{earth}} - t_{\mathrm{soi}_{\mathrm{from}}\mathrm{moon}} \tag{107}$$

It is claimed that this initial estimate procedure will yield errors that are within the convergence envelope of a simple differential correction procedure. This is verified numerically using a sample set of starting conditions and data.

VI. Differential Correction of the Infeasible Initial Estimate

The ease of convergence from the initial estimate, generated by the procedure described here, to a feasible solution is illustrated by the use of a differential correction procedure. Given the constraint vector $\mathbf{c}$ of dimension $m \times 1$ and the variable vector $\mathbf{x}$ of dimension $n \times 1$, the differential of the constraint vector is calculated from

$$\delta\mathbf{c} = \frac{\partial\mathbf{c}}{\partial\mathbf{x}}\delta\mathbf{x} \tag{108}$$

where the Jacobian matrix

$$\mathbf{J} = \frac{\partial\mathbf{c}}{\partial\mathbf{x}} \tag{109}$$

of size $m \times n$ is computed numerically using central differences.

The vector of variables for the one- and three-impulse TEI transfer sequence, and the constraint vector used in these simulations are

$$\mathbf{x}_{\mathrm{TEI}_1} = \begin{pmatrix} t_e \\ \mathbf{r}_{t_e} \\ \mathbf{v}_{t_e} \\ t_{\mathrm{soi}_{\mathrm{earth}}} \\ t_{\mathrm{soi}_{\mathrm{moon}}} \\ t_1 \\ \Delta\mathbf{v}_1 \end{pmatrix} \qquad \mathbf{x}_{\mathrm{TEI}_3} = \begin{pmatrix} t_e \\ \mathbf{r}_{t_e} \\ \mathbf{v}_{t_e} \\ t_{\mathrm{soi}_{\mathrm{earth}}} \\ t_{\mathrm{soi}_{\mathrm{moon}}} \\ t_1 \\ \Delta\mathbf{v}_1 \\ t_2 \\ \Delta\mathbf{v}_2 \\ t_3 \\ \Delta\mathbf{v}_3 \end{pmatrix}_{21\times 1} \tag{110}$$

$$\mathbf{c} = \begin{pmatrix} \Delta\mathbf{r}_{\mathrm{soi}} \\ \Delta\mathbf{v}_{\mathrm{soi}} \\ \Delta t_{\mathrm{soi}} \\ h_{t_e} - h_{t_e}^\star \end{pmatrix}_{8\times 1}$$

where $h_{t_e}^\star$ is a specified altitude at the Earth entry interface; here, a value of 121.9 km is used for $h_{t_e}^\star$, which is typical for an entry interface altitude for these types of missions. Though the procedure can also constrain the other set of Earth entry interface variables, only the altitude is constrained in place of the radial distance in the simulations presented here. For example, it is recalled that the initial estimate produces a zero flight-path angle at the Earth entry interface point. It is assumed that the solution that is continuous in the state at the mismatch time t_{soi} is nearby and that the flight-path angle along with the other entry interface variables do not change considerably between the initial estimate and the feasible solution.

A simple scaling of the variables and constraints is used. Where applicable, the time values $t_e, t_1, t_2, t_3, t_{\mathrm{soi}_{\mathrm{earth}}}$, and $t_{\mathrm{soi}_{\mathrm{moon}}}$ are scaled by 6.0, 1.0, 1.0, 1.0, 2.0, and 2.0 days, respectively; $\mathbf{r}_{\mathrm{te}}$ is scaled by 7000 km and $\mathbf{v}_{\mathrm{te}}$ is scaled by 12 km/s; all impulsive maneuver components in $\Delta\mathbf{v}_1, \Delta\mathbf{v}_2, \Delta\mathbf{v}_3$ are scaled by 1.6 km/s. The scales on $\Delta\mathbf{r}_{\mathrm{soi}}$, $\Delta\mathbf{v}_{\mathrm{soi}}$, Δt_{soi}, and $(h_{t_e} - h_{t_e}^\star)$ are 90,000 km, 1.6 km/s, 1.5 days, and 7000 km, respectively. These are reasonable scale values that do not need to be exact and which have been found to work well for the differential correction procedure used. After this scaling, the perturbation step sizes on the variables are determined by

$$h_i = 10^{-6}(1 + |x_{i_s}|) \tag{111}$$

where h_i is the perturbation step size for the scaled variable x_{i_s} associated with the element i, x_i, of the variable vector $\mathbf{x}$. In the case where the number of constraints is lower than that of optimization variables ($m < n$), which is the case for an optimization problem, the Jacobian matrix $\mathbf{J}$ is not invertible. The differential correction procedure used here makes use of the pseudo inverse of $\mathbf{J}$ to calculate a solution that satisfies the constraints ($\mathbf{c} = \mathbf{0}$) but that is not necessarily optimal [6]. The iteration procedure is

$$\mathbf{x}^{(i+1)} = \mathbf{x}^{(i)} - \mathbf{J}^{\star(i)}\mathbf{c}^{(i)} \tag{112}$$

where

$$\mathbf{J}^{\star} = \mathbf{J}^{\top}(\mathbf{J}\mathbf{J}^{\top})^{-1} \tag{113}$$

is known as the pseudo inverse of $\mathbf{J}$. This approach is not designed to optimize a cost function but to generate a feasible solution that is close to the initial estimate, as $\mathbf{J}^{\star}$ is derived from the minimum norm solution [6].

To illustrate the performance of the algorithm, eleven simulations have been executed for different epochs and initial parking orbits around the moon, each using a one-maneuver and a three-maneuver sequence, and the results obtained are shown in Tables 1–11, with both the initial estimate (IE) and the feasible trajectory (FT). The relative declination of the $\mathbf{v}_{\infty}^{+}$ vector with respect to the initial parking orbit plane is also shown and is characteristic of the magnitude of the plane change. For these simulations, the periapsis altitude of the low lunar orbit is 100 km, which again is typical value for this type of mission.

Furthermore, there are cases where three maneuvers will lead to a greater cost in terms of Δv than the one-maneuver case. Indeed, it is recalled that in this differential correction procedure the solution is not optimized and, from experimentation, the three-impulse escape sequence from the moon obtained from the initial estimate algorithm is less efficient than the one-impulse escape sequence when the relative declination of $\mathbf{v}_{\infty}^{+}$ with respect to the initial parking orbit is less than about 20°. The feasible and converged trajectories of a

Table 1 Targeting performance for a one- and three-impulse moon-to-Earth trajectory[a]

	$\Delta\mathbf{r}_{\text{soi}}$, km	$\Delta\mathbf{v}_{\text{soi}}$, km/s	Δt_{soi}, days	Total Δv, km/s	Iterations
TEI-1 (IE)	50470.5	0.412168	1.75517	2.09192	0
TEI-1 (FT)	8.95262e − 06	9.91545e − 11	1.68425e − 16	2.08354	6
TEI-3 (IE)	45735.4	0.320334	1.3885	1.60298	0
TEI-3 (FT)	1.60207e − 05	4.53236e − 11	3.3685e − 16	1.60476	6

[a]Epoch 2015/2/8 00:00:00, $a = 1838$ km, $e = 0$, $i = 30°$, $\Omega = 150°$, $\omega = 0°$, $\nu = 0°$ (relative declination = 49.859°).

Table 2 Targeting performance for a one- and three-impulse moon-to-Earth trajectory[a]

	$\Delta\mathbf{r}_{\text{soi}}$, km	$\Delta\mathbf{v}_{\text{soi}}$, km/s	Δt_{soi}, days	Total Δv, km/s	Iterations
TEI-1 (IE)	54048.0	0.464998	1.5042	1.58699	0
TEI-1 (FT)	1.25884e − 05	1.03303e − 10	0	1.58460	5
TEI-3 (IE)	48780.4	0.355693	1.1388	1.55197	0
TEI-3 (FT)	8.35043e − 06	7.16452e − 11	0	1.55402	6

[a]Epoch 2018/1/1 00:00:00, $a = 1838$ km, $e = 0$, $i = 92°$, $\Omega = 20°$, $\omega = 0°$, $\nu = 0°$ (relative declination = 25.664°).

Table 3 Targeting performance for a one- and three-impulse moon-to-Earth trajectory[a]

	$\Delta\mathbf{r}_{\text{soi}}$, km	$\Delta\mathbf{v}_{\text{soi}}$, km/s	Δt_{soi}, days	Total Δv, km/s	Iterations
TEI-1 (IE)	50244.8	0.458485	1.53273	2.23480	0
TEI-1 (FT)	1.76383e − 05	2.014e − 10	0	2.23188	5
TEI-3 (IE)	46541.2	0.351299	1.19888	1.62467	0
TEI-3 (FT)	1.30016e − 05	1.12523e − 10	0	1.62805	7

[a]Epoch 2019/3/21, 00:00:00, $a = 1838$ km, $e = 0$, $i = 92°$, $\Omega = 20°$, $\omega = 0°$, $\nu = 0°$ (relative declination = −54.700°).

Table 4 Targeting performance for a one- and three-impulse moon-to-Earth trajectory[a]

	$\Delta\mathbf{r}_{\text{soi}}$, km	$\Delta\mathbf{v}_{\text{soi}}$, km/s	Δt_{soi}, days	Total Δv, km/s	Iterations
TEI-1 (IE)	54952.4	0.399768	1.7191	2.51615	0
TEI-1 (FT)	1.13009e − 05	1.08261e − 10	0	2.50893	5
TEI-3 (IE)	50153.5	0.318606	1.36805	1.65684	0
TEI-3 (FT)	1.465e − 05	1.21773e − 10	0	1.65858	6

[a]Epoch 2020/12/25, 00:00:00, $a = 1838$ km, $e = 0$, $i = 92°$, $\Omega = 20°$, $\omega = 0°$, $\nu = 0°$ (relative declination = 69.087°).

Table 5 Targeting performance for a one- and three-impulse moon-to-Earth trajectory[a]

	$\Delta\mathbf{r}_{\text{soi}}$, km	$\Delta\mathbf{v}_{\text{soi}}$, km/s	Δt_{soi}, days	Total Δv, km/s	Iterations
TEI-1 (IE)	56293.9	0.415627	1.73016	1.40454	0
TEI-1 (FT)	2.2907e − 05	9.86511e − 11	0	1.39903	6
TEI-3 (IE)	53847.5	0.338046	1.39814	1.53701	0
TEI-3 (FT)	1.13939e − 05	1.49187e − 10	3.3685e − 16	1.54288	5

[a]Epoch 2034/2/8, 00:00:00, $a = 1838$ km, $e = 0$, $i = 153°$, $\Omega = 127°$, $\omega = 0°$, $\nu = 0°$ (relative declination = −12.968°).

Table 6 Targeting performance for a one- and three-impulse moon-to-Earth trajectory[a]

	$\Delta\mathbf{r}_{soi}$, km	$\Delta\mathbf{v}_{soi}$, km/s	Δt_{soi}, days	Total Δv, km/s	Iterations
TEI-1 (IE)	53645.4	0.397695	1.71596	2.43023	0
TEI-1 (FT)	4.93411e − 06	5.24529e − 11	0	2.42294	5
TEI-3 (IE)	50031.0	0.316343	1.35787	1.65542	0
TEI-3 (FT)	1.69956e − 05	1.4758e − 10	−3.3685e − 16	1.65777	6

[a]Epoch 2020/12/25, 00:00:00, $a = 1935$ km, $e = 0.05$, $i = 92°$, $\Omega = 20°$, $\omega = 0°$, $\nu = 0°$ (relative declination = 69.087°).

Table 7 Targeting performance for a one- and three-impulse moon-to-Earth trajectory[a]

	$\Delta\mathbf{r}_{soi}$, km	$\Delta\mathbf{v}_{soi}$, km/s	Δt_{soi}, days	Total Δv, km/s	Iterations
TEI-1 (IE)	52828.1	0.395853	1.71123	2.34176	0
TEI-1 (FT)	6.7731e − 07	1.15143e − 11	0	2.33453	5
TEI-3 (IE)	49893.8	0.313814	1.34648	1.66258	0
TEI-3 (FT)	1.51383e − 05	1.40514e − 10	0	1.6648	5

[a]Epoch 2020/12/25, 00:00:00, $a = 2043$ km, $e = 0.1$, $i = 92°$, $\Omega = 20°$, $\omega = 0°$, $\nu = 0°$ (relative declination = 69.087°).

Table 8 Targeting performance for a one- and three-impulse moon-to-Earth trajectory[a]

	$\Delta\mathbf{r}_{soi}$, km	$\Delta\mathbf{v}_{soi}$, km/s	Δt_{soi}, days	Total Δv, km/s	Iterations
TEI-1 (IE)	51297.4	0.391923	1.69974	2.15542	0
TEI-1 (FT)	9.89913e − 06	7.95526e − 11	0	2.14864	5
TEI-3 (IE)	49564.6	0.307782	1.31939	1.69818	0
TEI-3 (FT)	2.23197e − 05	2.00041e − 10	0	1.69988	5

[a]Epoch 2020/12/25, 00:00:00, $a = 2298$ km, $e = 0.2$, $i = 92°$, $\Omega = 20°$, $\omega = 0°$, $\nu = 0°$ (relative declination = 69.087°).

Table 9 Targeting performance for a one- and three-impulse moon-to-Earth trajectory[a]

	$\Delta\mathbf{r}_{soi}$, km	$\Delta\mathbf{v}_{soi}$, km/s	Δt_{soi}, days	Total Δv, km/s	Iterations
TEI-1 (IE)	50577.1	0.389674	1.69248	2.06105	0
TEI-1 (FT)	8.57914e − 06	6.90101e − 11	0	2.05452	5
TEI-3 (IE)	49359.4	0.304077	1.30295	1.72375	0
TEI-3 (FT)	3.25608e − 05	2.95887e − 10	0	1.72517	5

[a]Epoch 2020/12/25, 00:00:00, $a = 2451$ km, $e = 0.25$, $i = 92°$, $\Omega = 20°$, $\omega = 0°$, $\nu = 0°$ (relative declination = 69.087°).

Table 10 Targeting performance for a one- and three-impulse moon-to-Earth trajectory[a]

	$\Delta\mathbf{r}_{soi}$, km	$\Delta\mathbf{v}_{soi}$, km/s	Δt_{soi}, days	Total Δv, km/s	Iterations
TEI-1 (IE)	49850.6	0.387105	1.68387	1.96764	0
TEI-1 (FT)	8.46193e − 06	6.89069e − 11	0	1.96132	5
TEI-3 (IE)	49113.9	0.299719	1.28398	1.75292	0
TEI-3 (FT)	4.40276e − 05	4.02098e − 10	3.3685e − 16	1.75407	5

[a]Epoch 2020/12/25, 00:00:00, $a = 2626$ km, $e = 0.3$, $i = 92°$, $\Omega = 20°$, $\omega = 0°$, $\nu = 0°$ (relative declination = 69.087°).

Table 11 Targeting performance for a one- and three-impulse moon-to-Earth trajectory[a]

	$\Delta\mathbf{r}_{soi}$, km	$\Delta\mathbf{v}_{soi}$, km/s	Δt_{soi}, days	Total Δv, km/s	Iterations
TEI-1 (IE)	46118.2	0.371445	1.62921	1.61635	0
TEI-1 (FT)	4.7793e − 06	4.22552e − 11	0	1.61048	5
TEI-3 (IE)	47125.1	0.268437	1.16573	1.89067	0
TEI-3 (FT)	8.0038e − 05	7.51148e − 10	0	1.88983	5

[a]Epoch 2020/12/25, 00:00:00, $a = 3676$ km, $e = 0.5$, $i = 92°$, $\Omega = 20°$, $\omega = 0°$, $\nu = 0°$ (relative declination = 69.087°).

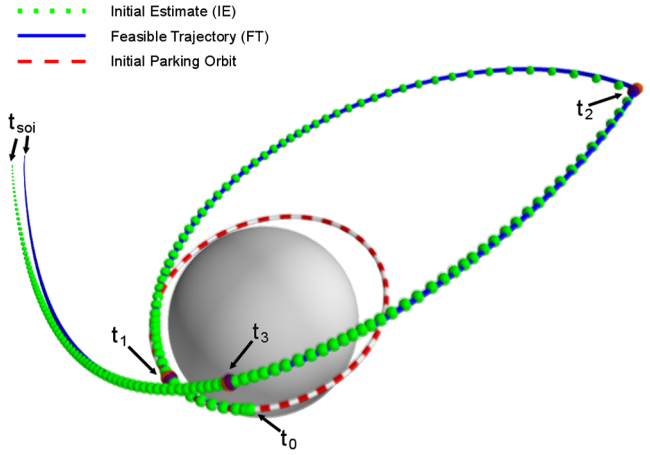

Fig. 3 Three-impulse TEI trajectory in moon-centered coordinates showing the IE and the feasible trajectory FT. The trajectories begin at t_0 and end at t_{soi} as shown. The three-maneuver times are t_1, t_2, and t_3, respectively. Though the times and locations of the maneuvers between these trajectories are different, they are nearly indistinguishable in the figure.

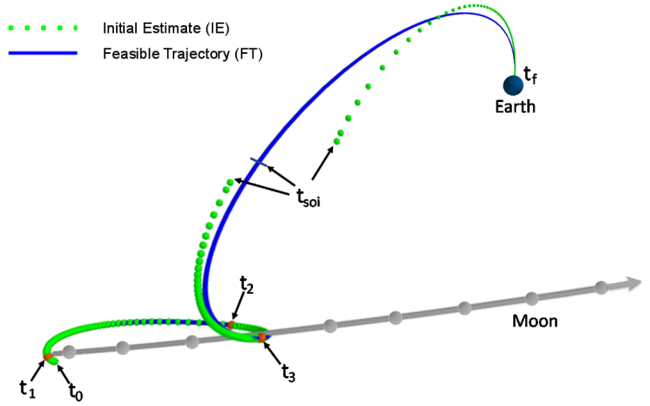

Fig. 4 Three-impulse TEI trajectory in Earth-centered coordinates showing the initial estimate IE and the feasible trajectory FT. The trajectories begin at t_0. The three-maneuver times and locations (which are nearly indistinguishable in the figure) are labeled as t_1, t_2, and t_3, respectively. The forward propagated trajectories from the moon end at t_{soi}. The backward propagated trajectories from the Earth begin at t_f and end at t_{soi}.

simulated example are shown in Figs. 3 and 4. Figure 3 shows a three-impulse TEI escape in moon-centered coordinates and Fig. 4 the complete trajectories in Earth centered coordinates.

VII. Conclusions

To examine the any-time abort capability required for a human lunar mission, a vector based analytical procedure has been developed to generate an initial trajectory model for a moon-to-Earth return trajectory that lies within the convergence envelope of a minimum norm differential correction procedure. The convergence to a feasible solution from typical input conditions can be achieved in a few iterations; typically seven or less for the examples presented.

If this algorithm is to be flown onboard a spacecraft and there is no ground link or onboard optimization capability, then at a minimum a feasible solution is available. If optimization capability is available, then the solution generated with the method described here serves as its initial estimate. The optimization of the impulsive maneuvers for the moon-centered escape phase of the problem has recently been analyzed by using a constrained optimization algorithm coupled with a state transition matrix based variational model to obtain the gradients of the problem functions with respect to the problem variables [7]. The initial estimate in that study was based on the procedure described here to construct the moon-centered escape sequence to a fixed relative hyperbolic excess velocity vector. Though the procedure described here provides a feasible one- or three-impulse solution for all relative declinations of the hyperbolic excess velocity vector, improvements are currently being investigated to produce feasible solutions for the escape phase that are closer to the optimal impulsive solution. A criteria should also be formulated, if possible, that indicates whether to use a one- or a three-impulse escape sequence (assuming those are the only two cases being considered). This may lead to the formulation of a more general set of criteria for one to maybe even four impulse escape sequences. It is clear that this is not necessarily a trivial problem when parameters such as the initial orbit eccentricity; radius and time constraints on locations of the maneuvers; and the relative right ascension of the hyperbolic excess velocity vector with respect to the periapsis vector of the initial orbit are considered.

The optimization of finite burn maneuvers with the constraint that each maneuver be required to be steered in a fixed plane but whose orientation for each maneuver forms part of the problem variables has also been examined using a constrained optimization algorithm with a state transition matrix based gradient calculation procedure [8]. All of these studies have as a final objective the development of a fully automated and robust procedure for constructing optimal high-fidelity moon-to-Earth trajectories for spacecraft equipped with either constant or variable exhaust velocity engines.

Acknowledgment

The authors wish to thank Gerald Condon of the NASA Johnson Space Center for serving as the technical supervisor of NASA grant NNX08AN02G, which supported part of this research.

References

[1] Gobetz, F. W., and Doll, J. R., "A Survey of Impulsive Trajectories, Final Report," United Aircraft Research Laboratories, Tech. Rept. G- 910557-11, 1968, pp. 17–20.

[2] Gunther, P., "Asymptotically Optimum Two-Impulse Transfer from lunar Orbit," *AIAA Journal*, Vol. 4, No. 2, 1966, pp. 346–352. doi:10.2514/3.3438

[3] Gerbracht, R. J., and Penzo, P. A., "Optimum Three-Impulse Transfer Between an Elliptic Orbit and a Non-Coplanar Escape Asymptote," *AAS/AIAA Astrodynamics Specialist Conference*, American Astronomical Society Paper 68-084, Jackson, WY, Sept. 1968.

[4] Bean, W. C., "Minimum ΔV, Three-Impulse Transfer Onto a Trans-Mars Asymptotic Velocity Vector," NASA TN D-5757, April 1970.

[5] Edelbaum, T. N., "Optimal Nonplanar Escape from Circular Orbits," *AIAA Journal*, Vol. 9, No. 12, 1971, pp. 2432–2436. doi:10.2514/3.50047

[6] Tapley, B. D., Schutz, B. E., and Born, G. H., *Statistical Orbit Determination*, Elsevier Academic Press, New York, 2004, p. 175.

[7] Ocampo, C., and Munoz, J.-P., "Variational Equations for a Generalized Spacecraft Trajectory Model," *19th AAS/AIAA Spaceflight Mechanics Meeting*, American Astronomical Society Paper 09-255, Savannah, GA, February 2009.

[8] Ocampo, C., and Munoz, J.-P., "Variational Model for the Optimization of Constrained Finite-Burn Escape Sequences," *AAS/AIAA Astro dynamics Specialist Conference*, American Astronomical Society Paper 09-381, Pittsburgh, PA, August 2009.